https://doi.org/10.5194/amt-2020-220
Preprint. Discussion started: 18 September 2020

Atmospheric Measurement Techniques
Discussions

Resolving ambiguous direction of arrival of weak meteor radar trail echoes

Daniel Kastinen[1,2], Johan Kero[1], Alexander Kozlovsky[3], and Mark Lester[4]

[1]Swedish Institute of Space Physics (IRF), Box 812, SE-98128 Kiruna, Sweden
[2]Umeå University, Department of Physics, SE-90187 Umeå, Sweden
[3]Sodankylä Geophysical Observatory, Sodankylä, Finland
[4]Department of Physics and Astronomy, University of Leicester, Leicester, United Kingdom

Correspondence: Daniel Kastinen (daniel.kastinen@irf.se)

Abstract. Meteor phenomena cause ionized plasmas that can be roughly divided into two distinctly different regimes: a dense and transient plasma region co-moving with the ablating meteoroid and a trail of diffusing plasma left in the atmosphere and moving with the neutral wind. Interferometric radar systems are used to observe the meteor trails and determine their positions and drift velocities. Depending on the spatial configuration of the receiving antennas and their individual gain patterns, the voltage response can be the same for several different plane wave Directions Of Arrival (DOA), thereby making it impossible to determine the correct direction. Noise can create the same effect even if the system contains no theoretical ambiguities. We propose a method for interferometric meteor trail radar data analysis using temporal integration of the signal spatial correlation to resolve DOA ambiguities. We have validated the method by a combination of Monte Carlo simulations and application on 10 minutes of measurement data (174 meteor events) obtained with the Sodankylä Geophysical Observatory SKiYMET all-sky interferometric meteor radar. We also applied a Bayesian method to determine the true location of ambiguous events in the data set. In 26 out of 27 ($\sim$96%) ambiguous cases, the temporally integrated spatial correlation gave the correct output DOA as determined by Bayesian inference. In the one case that was mis-classified there were not enough radar pulses to temporally integrate for the method to be effective.

1 Introduction

Every day the Earth's atmosphere is bombarded by billions of dust-sized particles and larger pieces of material from space. In doing so these objects, called meteoroids, ablate and produce phenomena called meteors (Ceplecha et al., 1998). These phenomena are commonly seen as visible streaks of light on the night sky.

Meteor phenomena cause ionized plasmas that can be roughly divided into two distinctly different regimes: a dense and transient plasma region co-moving with the ablating meteoroid and a trail of diffusing plasma left in the atmosphere and moving with the neutral wind. Both of these plasmas reflect radio waves. When measured with a radar, they cause so-called

https://doi.org/10.5194/amt-2020-220
Preprint. Discussion started: 18 September 2020

Atmospheric Measurement Techniques Discussions

meteor head and meteor trail echos (Kero et al., 2019). To determine the position of these radar targets, interferometric or multi-static radar systems must be used.

Observing this incoming material is important for several reasons. To mention a few: it gives us a unique opportunity to examine the motion and population of small bodies in the solar system (Vaubaillon et al., 2005a, b; Kastinen and Kero, 2017); it provides information about the extraterrestrial input of material into our atmosphere (Plane, 2012; Brown et al., 2002); it provides a possibility to assess the neutral wind at an altitude otherwise difficult to probe (Holdsworth et al., 2004; Hocking, 2005). The typical ablation altitude where meteor phenomena occur lie between 70 and 130 km (Kero et al., 2019, and references therein). This region is characterized by variability driven by atmospheric tides as well as planetary and smaller scale gravity waves. As this region is difficult to observe with other methods due to the low atmospheric density and high altitude, specular meteor trail radars have become widespread scientific instruments to study atmospheric dynamics. The extraterrestrial input of matter also affects various physical and chemical processes important for a wide range of phenomena, such as the formation of clouds at 15-25 km altitude responsible for ozone destruction in the polar regions, mid-latitude ice clouds at 75-85 km which are possible tracers of global climate change, and metallic ion layers in the atmosphere (Plane, 2003).

The diffusing meteor trail is an elongated plasma and not a point target. Therefore, specular reflection dominates. This makes interferometric all-sky radar systems efficient at observing the meteor trail phenomena with relatively inexpensive hardware. This has made such systems widespread and there are currently systems deployed at locations covering latitudes from Antarctica to the Arctic (Kero et al., 2019). When determining the position of an object by interferometry, there may be an ambiguity problem (Schmidt, 1986). The position is determined by finding the Direction Of Arrival (DOA) of the incoming echo onto the radar. Depending on the spatial configuration of the receiving antennas and their individual gain patterns, the voltage responses can be the same for several different plane wave DOA's, thereby making it impossible to determine which one is correct. Noise can create the same effect even if the system contains no theoretical ambiguities. These ambiguities then appear with a probability that is a function of the Signal to Noise Ratio (SNR) (Kastinen and Kero, 2020; Jones et al., 1998). This problem is general to all DOA determinations made by radar systems.

Due to its simplicity and theoretically unambiguous meteor trail position determination capability, the so-called Jones 2.5λ radar design has become the standard for specular meteor trail radars (Jones et al., 1998). However, it has been noted by several authors that if the SNR is low enough the position determination is still ambiguous (Jones et al., 1998; Hocking, 2005; Kastinen and Kero, 2020). For this reason, the widespread SKiYMET system has implemented a variable in their database referred to as `ambig` which gives several possible position solutions for the same event. A relatively small part of the total number of detected echoes have these angular ambiguities, generally around 10-20% (Fig. 3a Hocking et al., 2001). Practically, these type of events cannot be used for wind determination as correct location is needed in order to determine the line-of-sight direction for the wind component estimation. Meteroid radiants can also not be determined if the location is ambiguous. Therefore it is important, not only to improve the quality of atmospheric wind measurements, but also for meteor research to resolve the ambiguity issue.

Chau and Clahsen (2019) examined the morphology of ambiguities for the Jones 2.5λ design and other radar systems using the beamforming Point Spread Function (PSF). In the case of radars with identical antenna elements, each having a separate

https://doi.org/10.5194/amt-2020-220
Preprint. Discussion started: 18 September 2020

Atmospheric Measurement Techniques Discussions

signal channel, the PSF is identical for all input DOAs. The identification done in Chau and Clahsen (2019) thereby apply for all input DOA.

It should be noted that for systems with non-identical gain patterns for each channel, e.g. radars with dissimilar or asymmetric antenna subarrays, or non-planar arrays the PSFs will change as a function of input DOA. Detailed simulations of this ambiguity problem were performed in Kastinen and Kero (2020) and Bayesian methods to infer the true DOA of ambiguous data were presented.

The PSF reported in Chau and Clahsen (2019, Fig. 1) match with the morphology of the Monte-Carlo simulations of DOA determination performed here and in Kastinen and Kero (2020). Given a Bayesian method to assign probability distributions to the ambiguities, many of the previously unusable data may be again usable. Events with high certainty in inference of the true DOA provide a validation for methods to resolve the ambiguity in the analysis itself without simulations.

We propose a method to use temporal integration of the signal spatial correlation to resolve DOA ambiguities. We validate the method by application on measurement data in parallel with simulation and application of a Bayesian method to determine the true location. The temporal integration method is defined to succeed if the DOA by the Bayesian method is given a very high probability of being true. Temporal integration is possible in the case of meteor trail echoes as the drift velocity due to the neutral wind and the range from the ground to the meteor zone makes the angular change in time small compared to the temporal integration window.

Holdsworth et al. (2004) implemented a coherent detection algorithm where linear regression was applied on the measured cross correlation angles. A linear regression is more sensitive to outliers and noise then temporal integration of complex amplitudes, but it does take into account a possible drift of the target as a function of time. However, considering the small typical drift speeds of meteor trails compared to the range, temporal integration of complex amplitudes ought to be more stable for low SNR events.

When we temporally integrate spatial cross correlations of a virtually stationary plane wave, the integration is coherent. However, a more effective coherent integration would be to apply a matched filter and coherently integrate prior to calculating the cross correlation.

We have elected not to implement a matched filter routine for the SKiYMET system as that is outside the scope of this study. A simple derivation of the effectiveness and coherence of these two temporal integration techniques is given in Appendix A.

2 Instrumentation

2.1 System

We use data from the meteor radar at Sodankylä Geophysical Observatory (SGO, 67° 22’ N, 26° 38’ E, Finland). The radar is an all-sky interferometric meteor radar SKiYMET operating at a frequency of 36.9 MHz. The power of the radar transmission is 15 kW (upgraded from 7.5 kW in September 2009). The Pulse Repetition Frequency (PRF) is 2144 Hz. The width of each pulse is 13 µs, which gives a range resolution (size of the range bins) of 2 km. The five-antenna receiving array is arranged as an interferometer, and phase differences in the signals arriving at each of the antennas of the interferometer are used to determine

https://doi.org/10.5194/amt-2020-220
Preprint. Discussion started: 18 September 2020

a theoretically unambiguous angle of arrival. This allows the determination of meteor echo azimuth and elevation angles to an accuracy of about 1° (Jones et al., 1998). Also, the receiving system determines the Doppler velocity of the selected targets. Details of the SKiYMET radar system and algorithms of the radar signal processing are described in Hocking et al. (2001).

2.2 Database

An important task of the standard SKiYMET real-time signal processing is selecting meteor echoes and rejecting other signals, such as echoes from satellites and aircraft, lightning, and sporadic ionospheric layers. The characteristic features used to distinguish meteor echoes from other signals include their rapid onset, relatively short duration (typically less than $0.3\ \mathrm{s}$), and quasi-exponential decay. Only echoes with SNR>2 dB are accepted by the system.

In the routine meteor radar operations, short $4\ \mathrm{s}$ records of the signals (real and imaginary components) received at each of the five antennas are analyzed and archived as Confirmed Events (CEV) data files for each echo accepted as a meteor (i.e., "event"). Because of the coherent integration over four subsequent counts, the sampling rate of CEV data is $536\ \mathrm{Hz}$. Examples of such records are presented in Sect. 5.

For the targets selected by the system as meteors, their position (azimuth, elevation, range, and height), Doppler velocity of the scatter from these targets, and the decay time of the scatter from the targets are determined. These parameters are stored in the Meteor Position Data (MPD) files.

Each MPD file corresponds to a 24-hour time span starting at 0000 UTC and ending at 2359.59 UTC the same day. For unambiguous targets, one line per meteor detection is recorded. If a meteor cannot be unambiguously located, all various possible locations are reported in the MPD file with one line per ambiguous location. This is noted in the " AMBIG" field of the data. If the AMBIG field is 3, for example, then there will be three consecutive entries in the MPD file for this one meteor. There may be ambiguities in both range and/or DOA. The PRF of subsequent transmissions is $2144\ \mathrm{Hz}$, which means that the range is determined with a $\sim 70\ \mathrm{km}$ ambiguity. To reduce the range ambiguity, the SKiYMET data analysis algorithm assumes that meteor trails are located at heights between 70 and $110\ \mathrm{km}$.

In the present study we used data collected on 13 December 2018 between 0000 and 0010 UTC. In these 10 minutes of data there were 175 recorded events. Of these events, 31 ($\sim$18%) contained angular ambiguities indicated in the MPD file. We discovered that one event had been divided into two separate events in the database. Therefore, only 30 events were analysed.

3 Method

We have applied two separate methods for inferring the true location of an ambiguous DOA measurement. The first method is based on DOA determination direct Monte Carlo simulation and Bayesian inference and has been presented in Kastinen and Kero (2020). This method is complex and costly in terms of computation resources, but yields a probability distribution over the ambiguities. The second method is temporal integration of the spatial correlation matrix, described in detail in Sect. 3.2. This second method is easily implemented in data analysis pipelines and requires less computations then regular DOA determination.

The DOA determination performance investigation of the Jones 2.5λ radar presented by Kastinen and Kero (2020) successfully made use of the multiple signal classification (MUSIC) algorithm developed by Schmidt (1986). Holdsworth (2005) investigated the Jones antenna configuration and found that the usage of 2.5, 3 and 5.5λ spacings could produce more accurate echo DOA. Younger and Reid (2017) developed the concept further and presented a solution which utilises all possible antenna pairs of a meteor radar antenna configuration, similarly to the DOA calculations using the MUSIC algorithm. We have applied the same implementation of MUSIC as described by Kastinen and Kero (2020) to analyse the SKiYMET data in this study.

3.1 Sensor response model

The standard Jones type interferometer has five antennas, ideally identical, all with individual channels for recording complex voltage data. A model for this type of radar receiving a plane wave of amplitude A is described by

$$\mathbf{\Phi}(\mathbf{k}) = g(\mathbf{k}) \begin{pmatrix} Ae^{-i\langle \mathbf{k}, \mathbf{r}_1 \rangle_{\mathbb{R}^3}} \\ \vdots \\ Ae^{-i\langle \mathbf{k}, \mathbf{r}_N \rangle_{\mathbb{R}^3}} \end{pmatrix}. \quad (1)$$

Here the complex vector $\mathbf{\Phi}(\mathbf{k})$ is the the modeled set of complex voltages output by the radar system given the that the incoming wave DOA is $\mathbf{k}$. The $\mathbf{r}_i$ vectors represents spatial antenna locations and $g(\mathbf{k})$ the gain pattern of the antennas.

3.2 Spatial correlation matrix

We define a measured sensor response as the complex vector $\mathbf{x} \in \mathbb{C}^N$. The SKiYMET radar uses a single pulse transmission, i.e. no coded transmission sequences, without oversampling on reception. There is only a single temporal sample of the echo for each pulse. Therefore, the sensor response model in Eq. 1 directly models a received echo. The measurement vector $\mathbf{x}$ consists of the ideal response $\mathbf{\Phi}(\mathbf{k})$ and additive white noise $\boldsymbol{\xi}$(e.g Bianchi and Meloni, 2007; Polisensky, 2007),

$$\mathbf{x} = \mathbf{\Phi}(\mathbf{k}) + \boldsymbol{\xi}. \quad (2)$$

However, if the noise is spatially correlated the cross correlations between antennas can exhibit noise spikes at zeroth temporal lag (Holdsworth et al., 2004). Considering the setup of the system, any spatially correlated noise from galactic sources should be small enough not impact the main purpose of this study, as is discussed further in Appendix A.

Another possible effect on the sensor response is mutual coupling. It is known that mutual coupling introduce constant phase errors on the signals from individual antennas, resulting in zenith angle errors of up to 0.5° for the Jones configuration (Younger and Reid, 2017). We are not applying corrections specifically for mutual coupling phase errors, but we do apply the system phase calibration data given in the MPD file. This phase calibration data should include the effects of mutual coupling. Regardless, phase errors that are stationary as a function of time for a fixed beam pointing direction and pulse transmission sequence will not decorrelate the temporal integration of the spatial correlation matrix between IPPs. They will also not affect the ambiguity dynamics, as the gain pattern of all channels are identical.

https://doi.org/10.5194/amt-2020-220
Preprint. Discussion started: 18 September 2020

Atmospheric Measurement Techniques
Discussions

As such, we can assume that the white noise $\boldsymbol{\xi}$ is a complex circularly symmetric normal distribution for each dimension, i.e. $\boldsymbol{\xi} \sim \mathcal{CN}^N(0,\sigma^2)$ that is uncorrelated both in space and time. The spatial correlation matrix R of our measurements is calculated as

$$R = \mathbf{x}\mathbf{x}^\dagger. \tag{3}$$

The spatial correlation matrix contains the information of all possible phase differences between antennas as measured by the radar, as well as the signal power in the diagonal.

3.3 MUSIC

A detailed description of the MUSIC implementation we have used is given in Kastinen and Kero (2020). Here, we notate the entire process by a function G that takes as input the spatial correlation matrix R and the sensor response model $\boldsymbol{\Phi}(\mathbf{k})$. The function G outputs an estimated DOA $\tilde{\mathbf{k}}$ and the level at which the sensor response model matched the measured signal, F,

$$G(R,\boldsymbol{\Phi}) = (F,\tilde{\mathbf{k}}). \tag{4}$$

The quantity F describes the level to which the MUSIC implementation was able to match the used model $\boldsymbol{\Phi}$ with the measured signal $\mathbf{x}$, which we call the MUSIC response. If there is a perfect match $F \mapsto \infty$ while a total mismatch is represented by $F = 1$. We have here adopted the convention that Azimuth measures the angle counterclockwise from East.

3.4 Algorithm improvement

The key to the proposed improvement in ability to resolve angular ambiguities lies in the relatively slow drift speed of the trail echoes. The possible DOA change due to drift with the local wind over the typical dynamical lifetime of a meteor trail event is small. Therefore we can assume that the individual spatial correlation matrices for each measured radar pulse are practically statistical sample points of the same quantity. Consequently, this quantity can be temporally integrated to increase the SNR of each element of the matrix. The temporally integrated spatial correlation matrix is defined as

$$\bar{R} = \sum_{i=1}^{N_s} R_i, \tag{5}$$

where there are N_s measured pulses from the trail in question. The theoretical relation between coherent integrations N_s and SNR is SNR$\propto N_s$. Below, we sometimes refer to a set of N_s measured radar pulses as a number of Inter Pulse Periods (IPPs). Each IPP corresponds to ~ 466 µs of time, i.e. the inverse of the PRF.

The MUSIC response F is equivalent to SNR for DOA determination (Schmidt, 1986). Thus, as the MUSIC response $\bar{F}$ depends on the temporally integrated spatial correlation matrix $\bar{R}$ we expect $\bar{F} \propto N_s$. An example is illustrated in Fig. 1 where $\sim 1 \cdot 10^4$ echoes originating from 0° azimuth and 45° elevation were simulated at an SNR of 10 dB for the SKiYMET radar. These echoes were analysed with the MUSIC algorithm, G. Then, up to 200 of the spatial correlation matrices were temporally integrated and used as input to the MUSIC algorithm. The results are illustrated in the right column of the figure. Here,

https://doi.org/10.5194/amt-2020-220
Preprint. Discussion started: 18 September 2020

Atmospheric Measurement Techniques Discussions

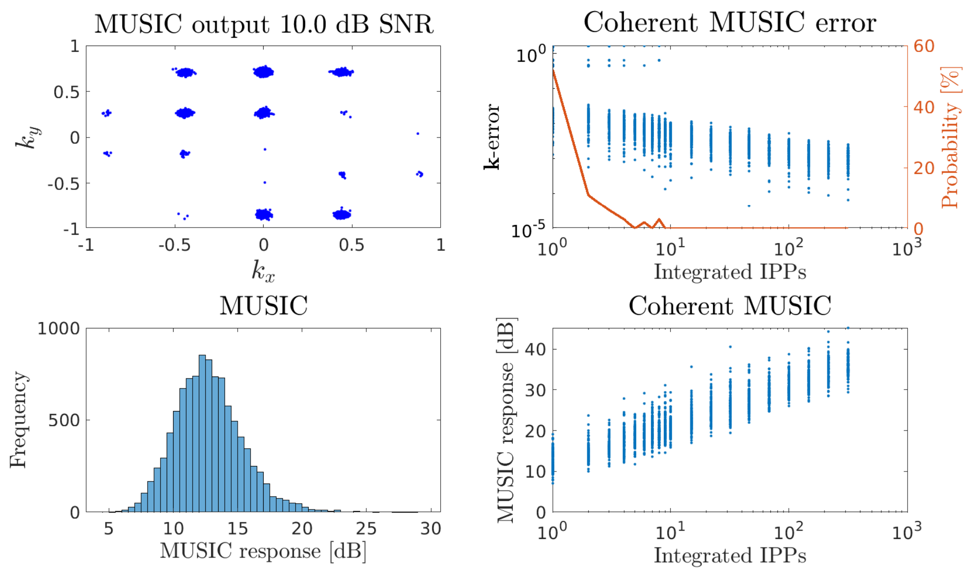

Figure 1. Example showing the effects on DOA determination using MUSIC when temporally integrating the spatial correlation matrix. $\sim 1 \cdot 10^4$ echoes originating from 0° azimuth and 45° elevation were simulated at an SNR of 10 dB for the SKiYMET radar system. These echoes were analysed with the MUSIC algorithm individually as well as up to 200 of the spatial correlation matrices were temporally integrated and analysed. In the upper left panel the MUSIC DOA output for the individual simulations are illustrated in the wave vector ground projection plane, i.e k_x, k_y. In the lower left panel the distribution of MUSIC responses are gathered as a histogram. The panels to the right display the results as a function of number of temporally integrated matrices. The MUSIC response is given in the lower panel and the wave vector error in the upper panel. Additionally, in the upper right panel on the right vertical axis, we illustrate the probability of ambiguous output. In this example, the probability drops significantly already with 2-3 integrated matrices and the ambiguous output DOA behaviour disappears completely after 10 integrated matrices.

as expected, one order of magnitude temporally integrated sample points correspond to a 10 dB MUSIC response increase. Additionally, in the upper right panel on the right vertical axis, we illustrate the probability of ambiguous output. In this example, the probability drops significantly already with 2-3 integrated matrices and the ambiguous output DOA behaviour disappears completely after 10 integrated matrices.

Even though this shows that SNR and MUSIC response is perfectly correlated, one must not mistake MUSIC response as a proxy for absolute precision of the angular determination. The MUSIC response function is the inverse of a scalar vector projection onto the noise subspace (Schmidt, 1986). The basis set of the noise subspace will vary depending on the noise in the signal. The implementation we have used of MUSIC sweeps all parameters of a sensor response model to find the sensor response with the smallest noise subspace component. This means that even though the noise subspace component of the output point would be small, the signal space could simply have been displaced to this point by the noise. Thus, the MUSIC response is not a direct indication of error but simply an indication of how well the sensor response model was able to match

https://doi.org/10.5194/amt-2020-220
Preprint. Discussion started: 18 September 2020

Atmospheric Measurement Techniques Discussions

the measured signal subspace. Hence, the mean of the distribution of MUSIC responses increases with SNR but is uncorrelated with the true angular error.

4 Simulation

4.1 Direct Monte Carlo

As outlined in Kastinen and Kero (2020), direct Monte Carlo (MC) simulations of DOA determinations can resolve the ambiguity dynamics of a radar system. Such MC DOA determination simulations are shown in Fig. 1. Using such simulations, one can match the measured ambiguity pattern with a simulated theoretical one to infer the true DOA of an ambiguous measurement.

4.2 Bayesian inference

The matching process of comparing a simulated DOA output distribution with a measured one can be done by hand. Ideally, a quantitative and algorithmic approach should be used. Kastinen and Kero (2020) showed that a Bayesian approach is a suitable way to perform systematic and quantitative matching of simulations to observations. We have implemented a modified version of the method outlined there.

Given a model with parameters $\mathbf{y}$ which has generated observations D, Bayesian inference can be used to find the probability distribution of possible model parameters. This distribution is called the posterior $\mathcal{P}(\mathbf{y})$. The posterior is connected to a prior probability $\theta(\mathbf{y})$, i.e. what we think the distribution is before any observations. The observed data is used to update the prior distribution by use of a likelihood function L. This likelihood function determines how probable the observed data D is given the model parameters $\mathbf{y}$. The relationship between the prior θ, likelihood L and posterior $\mathcal{P}$ is given by Bayes' theorem,

$$\mathcal{P}(\mathbf{y}) = \frac{L(D|\mathbf{y})\theta(\mathbf{y})}{\int L(D|\mathbf{y}')\theta(\mathbf{y}')\mathrm{d}\mathbf{y}'}. \tag{6}$$

Here $|$ indicates conditional probability. In our application, the model parameters $\mathbf{y}$ are the ambiguous DOA locations labeled by an index $\mathbf{y} = j$.

The Bayesian approach in Kastinen and Kero (2020) used individual DOA measurements and multinomial sequence generation probabilities to infer the true location. Their approach was designed considering low number statistics, i.e. on the order of 10 independent measurements. The SKiYMET system has a high PRF compared to the typical experimental setups at several of the radar systems that were examined in Kastinen and Kero (2020). Usually, hundreds of received pulses are available from each meteor event. Practically, this makes the discrete sequence Bayesian approach unstable if the simulations do not exactly model the probability of algorithm failure. Modeling this probability is very costly in terms of computational resources. However, as there are generally hundreds of measured sample points one can instead calculate the multinomial distribution itself with high accuracy. The measured multinomial distribution can then be directly compared with the simulated multinomial distribution. A detailed account of how to discretize the DOA distribution into a multinomial distribution was given in Kastinen

https://doi.org/10.5194/amt-2020-220
Preprint. Discussion started: 18 September 2020

and Kero (2020). The description includes both how multinomial probabilities are generated from the MC simulations, here denoted $\hat{P}_{ij}$, and probabilities calculated from measurements, denoted $\tilde{P}_i$. The index i denotes a possible ambiguous DOA location while the index j denotes the true location. As an example, the notation $\hat{P}_{12} = 0.25$ would mean that there is a 25% probability that ambiguity location 1 is the output from a measurement generated by a target at location labeled 2 (given the specific SNR in the simulation).

In the current modified Bayesian inference approach we redefine the likelihood function in terms of simulated and measured multinomial parameters. We regard the simulated multinomial parameters as exact and true. The measured multinomial parameters are found by calculating the probabilities

$$P_i = P(\tilde{\mathbf{k}} \in A_i) \approx \tilde{P}_i = \frac{1}{N_s} \sum_{l=1}^{N_s} \begin{cases} 1 & \text{if } \tilde{\mathbf{k}}_l \in A_i \\ 0 & \text{if } \tilde{\mathbf{k}}_l \notin A_i \end{cases}, \tag{7}$$

where A_i is the region for an ambiguous DOA. This is identical to computing the expected value of 1 over the measured sample points, or calculating the multinomial maximum likelihood estimator. Given enough sample points, the central limit theorem applies and the multinomial probability estimator can be regarded as normal. It is therefore equivalent to the Bernoulli mean estimator distribution. The estimator variance can be approximated by substituting the distribution variance with the measured Bernoulli variance (Papoulis and Pillai, 2002),

$$\mathrm{var}(\tilde{P}_i) \approx \frac{\tilde{P}_i(1 - \tilde{P}_i)}{N_s}. \tag{8}$$

For the special case of $\tilde{P}_i = 0$ (corresponding to no measurements in an inclusion region A_i) we have implemented an estimator variance similar to the considerations in Hanley and Lippman-Hand (1983) and defined $\mathrm{var}(\tilde{P}_i) = -\frac{\ln(0.05)}{2N_s}$. Then, the modified likelihood function can be written in log form as

$$\ln(L(j)) = \sum_{i=1}^{N_o} -\ln\left(\sqrt{\mathrm{var}(\tilde{P}_i)2\pi}\right) - \frac{1}{2}\frac{(\hat{P}_{ij} - \tilde{P}_i)^2}{\mathrm{var}(\tilde{P}_i)}, \tag{9}$$

where N_o is the number of ambiguous regions.

To avoid contamination of the probabilities by faulty IPP selection, i.e selecting IPPs that do not contain a valid echo from the trail, we only use the ambiguous locations as parameters in the multinomial distribution and do not include an algorithm failure probability.

As we have no prior information on the location of the target, Bayes' theorem from Eq. 6 reduces to

$$\mathcal{P}(j) = \frac{L(j)}{\sum_j L(j)}. \tag{10}$$

5 Results

In total, 30 events were analysed with both the MC simulation based Bayesian inference and the temporal integration version of MUSIC. An example of such an event is illustrated in Fig. 2. The upper right panel illustrates SNR versus radar pulse, the two

https://doi.org/10.5194/amt-2020-220
Preprint. Discussion started: 18 September 2020

Atmospheric Measurement Techniques Discussions

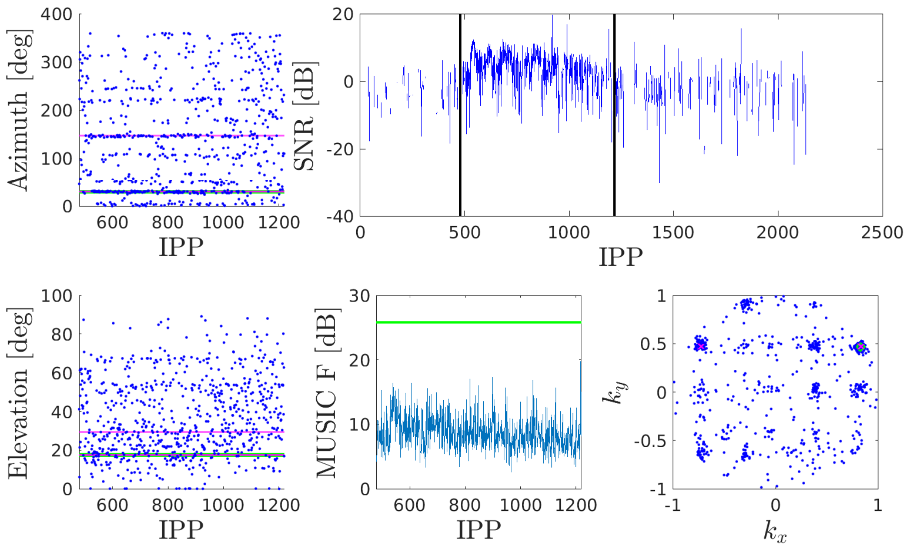

Figure 2. Meteor recorded at 2018-12-13 00:03:27.302 UTC. The upper right panel illustrates SNR versus IPP and the two vertical black lines denotes when the meteor occurred. This event had three range ambiguities: 187.9 km, 257.9 km and 327.9 km, and two angular ambiguities. The peak SNR was 8.7 dB. The two angular ambiguities are marked by red lines in the upper left panel (azimuth) and the lower left panel (elevation). The MUSIC DOA output from event IPPs are illustrated as blue dots and the green transparent line denotes the DOA output after temporal integration. The same information is given in wave vector ground projected space, k_x, k_y in the lower right panel. Here, the MPD-file ambiguities are marked by red crosses and the temporally integrated MUSIC by a green circle. Finally, the distribution of MUSIC responses F as a function of IPP is illustrated in the lower middle panel. Here, the green line denotes the MUSIC response for the temporally integrated spatial correlation matrix.

vertical black lines denotes the region within which the trail event was producing radar echoes. These are the pulses that were analysed using the MUSIC algorithm. The DOA output from these IPPs are illustrated as blue dots in the left column of panels. The upper left panel shows azimuth as a function of IPP and the lower one elevation. Here, the transparent red lines denote the azimuth and elevation given in the MPD-file. In this case, the standard SKiYMET analysis produced three angular ambiguities. The green transparent line denotes the DOA output from the temporal integration version of MUSIC. The same information is given in wave vector ground projected space, k_x, k_y in the lower right panel. Here the MPD-file results are marked by red crosses and the temporal integrated MUSIC by a green circle, while the regular MUSIC output for each IPP is marked by the blue dots. Finally, the distribution of the MUSIC response F is illustrated in the lower middle panel as a function of IPP. Here, the solid green line denotes the MUSIC response for the temporally integrated spatial correlation matrix.

For each of the 30 events we also performed a series of MC DOA determination simulations. The noise in the simulations was set to sample from the distribution of SNRs measured for the event themselves as to reproduce the multinomial probabilities. In Fig. 3, the simulations and the Bayesian inference results are illustrated alongside the measurement data for the event also

https://doi.org/10.5194/amt-2020-220
Preprint. Discussion started: 18 September 2020

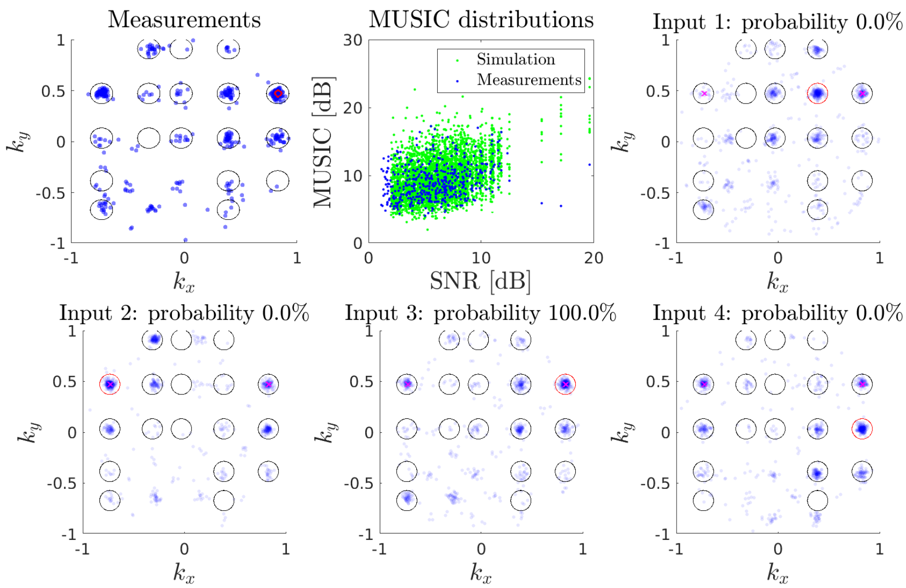

Figure 3. Summary of the DOA determination simulations and the Bayesian inference results for the meteor in Fig. 2. Four different possible true DOAs were identified and their individual MC simulations are illustrated in the panels titled Input 1-4. The Bayesian probability of an input DOA being the true location of the trail is given in the title. In each of these panels, the input DOA is marked by a large red circle and the MPD-file results are marked by red crosses. The measured DOA output distribution is given in the upper left panel. The black circles denote the possible ambiguities and their inclusion regions. The small red circle denotes the MUSIC output after temporal integration. The upper middle panel shows the measured and simulated distributions of MUSIC response F versus SNR.

illustrated in Fig. 2. The upper left panel shows the MUSIC DOA output in wave vector ground projected space, i.e. k_x and k_y. The black circles denote the possible ambiguities and their inclusion regions, i.e. the A_i sets from Eq. 7. The small red circle denotes the output from the temporally integrated MUSIC. The upper middle panel shows the measured distribution of SNR versus MUSIC response compared to the simulated distribution. The remaining panels show MC DOA determination simulations with different true inputs. In each of these panels, the input DOA is marked by the large red circle. For reference, the MPD-file results are also marked by transparent red crosses in each panel. The title of these figures give the Bayesian inference results $\mathcal{P}(j)$ in percent rounded to one decimal. The Bayesian inference can also be evaluated manually by comparing the simulated distribution of DOA outputs with the measurements given in the upper left panel. In this case, the Bayesian inference and the temporally integrated MUSIC, as well as a manual inspection, all agree and identify the same DOA as the true location.

Of the 30 analysed events, 26 were correctly identified with the temporal integration version of MUSIC. Two of the cases not correctly identified were on closer inspection noise erroneously identified as a meteor trail echo or an event too weak (SNR around 1-6 dB) to be analysable. In one of the remaining two cases, the simulations could not recreate the measured DOA distribution, and the other had too few IPPs available (less then 10 with SNR > 5 dB) for temporal integration to identify the

https://doi.org/10.5194/amt-2020-220
Preprint. Discussion started: 18 September 2020

Atmospheric Measurement Techniques Discussions

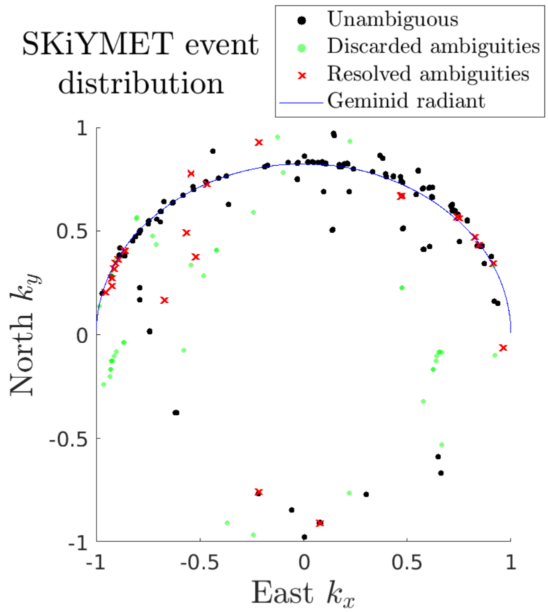

Figure 4. Illustration of the event distribution improvement in 10 minutes of Sodankylä SKiYMET meteor radar data after applying temporal integration. The black dots are the unambiguous meteor trail events, the green dots are the original ambiguous locations that could be discarded, and the red crosses are the resolved ambiguities after temporal integration. There are multiple green dots per event and red cross. The data was recorded during the Geminid meteor shower. The blue line illustrates directions that fulfill the specular condition for meteors arriving from the Geminid radiant.

correct DOA. To summarize: 27 of the 30 events could be validated and analysed with the Bayesian inference, and 26 of these ($\sim$96%) were correctly identified by temporal integration.

The DOA distribution for the 10 minutes of data is illustrated in Fig. 4. The black dots are the 144 unambiguous meteor trail events, the green dots are the original ambiguous locations that could be discarded, and the red crosses are the 26 resolved ambiguities after temporal integration. There are multiple green dots per resolved ambiguous event, i.e. red cross.

The DOA distribution is concentrated towards low elevation in the north, as this data was recorded during the Geminid meteor shower. The blue line shows the locations where specular reflection could occur assuming that the meteor originated from the centre of the Geminid meteor shower radiant region (right ascension 112°, declination 33°) at the time of the measurement.

At around 0 UTC, the Geminid radiant as well as most sporadic meteor source regions were located towards the south (Wiegert et al., 2009) since Sodankylä is located at a high northern latitude. Therefore, most meteors with trajectories fulfilling a specular condition with respect to the radar appeared towards the north. This explains the concentration of DOAs towards the north at low elevation in Fig. 4. As illustrated in the figure, the measured distribution was significantly improved after applying temporal integration of the spatial correlation matrix.

For five of the resolved angular ambiguities, the temporal integration also solved the range ambiguity. Eighteen still have two range ambiguities, one of them has three range ambiguities, and two did not have a range ambiguity to begin with. However,

https://doi.org/10.5194/amt-2020-220
Preprint. Discussion started: 18 September 2020

the range ambiguity would be easily avoided with an update of the system to use coded transmission sequences. An advanced example is give by Vierinen et al. (2016), who used coded transmission sequences with a Multiple Input Multiple Output bi-static and Continuous Wave setup. In the case of the mono-static Sodankylä SKiYMET system, it would be enough to use a small set of binary phase shift key codes on the pulsed transmitter to enable distinguishing the pulse trains that come from subsequent echoes within the meteor zone.

The problem with range ambiguities is independent from the angular ambiguity problem and outside the scope of this paper. The reason why range ambiguities appear in the standardized SKiYMET analysis is the combination of uncoded radar pulses and high PRF. At low elevation angles from the radar, this means that two or more consecutively transmitted pulses simultaneously may give rise to echoes of meteors in the standardized acceptable altitude range 70-110 km (Hocking et al., 2001). The commonly used PRF 2144 Hz of the SKiYMET radar systems corresponds to a range aliasing of $\simeq$ 70 km.

6 Conclusions

We have shown that a Bayesian inference approach systematically can determine the true location of weak meteor radar trail echoes with ambiguous DOA. To perform the Bayesian inference, extensive MC DOA determination simulations are required and this method is as such computationally expensive. However, the results were used to validate another method to resolve the ambiguous DOA.

We propose temporal integration of the spatial correlation matrix and subsequent application of the MUSIC algorithm as a computationally inexpensive and implementation-wise simple method to resolve ambiguous DOAs. The temporally integrated version of MUSIC provided the correct output DOA according to the Bayesian inference in 26 of 27 ($\sim$96%) of the test cases. In the case that was mis-classified, there were not enough sample points (12 points > 7 dB SNR and only 3 > 10 dB SNR) to temporally integrate for the method to be effective.

Standard meteor trail radar systems, such as SKiYMET (Hocking et al., 2001) generally produce enough sample points from each registered meteor for the temporally integrated MUSIC to work. The results indicate that this method will solve the angular ambiguity problem in almost all cases. The problem with range ambiguities is independent from the angular ambiguity problem and outside the scope of this paper, but could be avoided with an update of the system to use coded transmission sequences.

It is important to note that this method is not unique for use with the MUSIC algorithm: e.g. the complex signal amplitudes that are used in the DOA determination algorithm by Jones et al. (1998) to calculate the ϕ angles can be temporally integrated in the same way as the spatial correlation matrix R was temporally integrated here.

Data availability. The data described in Sect. 2.2 that was analysed, i.e the Confirmed Events (CEV) files and the Meteor Position Data (MPD) file, are included as supplementary material together with a short description of their structure.

https://doi.org/10.5194/amt-2020-220
Preprint. Discussion started: 18 September 2020

Atmospheric Measurement Techniques
Discussions

Appendix A: Temporal integration of cross correlations

Extending the definition used in Eqs. 1 and 2 to include temporal variations we define

$$\Phi_{j,n} = g_j(\mathbf{k}_n) A_n e^{-i(\langle \mathbf{k}_n, \mathbf{r}_j \rangle_{\mathbb{R}^3} - \phi_n)}, \tag{A1}$$

$$\tilde{\Phi}_{j,n} = \Phi_{j,n} + \xi_{j,n}, \tag{A2}$$

where n denotes the temporal component and the noise is $\xi_{j,n} \sim \mathcal{CN}(0, \sigma_n^2)$, i.e. a complex circularly symmetric normal random variable. Here $\mathbf{k}_n$ is the incident wave vector, A_n is the wave amplitude, $\langle , \rangle_{\mathbb{R}^3}$ is the inner product, $\mathbf{r}_j$ is the physical location of antenna j and g_j its gain pattern. We will assume that the noise is uncorrelated between samples of j and between samples of n. In reality, if there is a particularly strong point source of noise compared to the overall background noise, the total noise picked up by an antenna may become spatially correlated. There are galactic sources that produce such noise (Gaensler, 2004). However, given the low directivities of the SKiYMET antennas and the fact that it is a single-pulse system, assuming completely uncorrelated noise is acceptable for this derivation.

For simplicity, we will make the following further assumptions for Eq. A2: individual antenna gain is unity $g_j = 1$; signal amplitude is constant over antennas and time $A_n = A$; the wave vector change due to the local wind drift velocity over the meteor trail event time is negligible $\mathbf{k}_n = \mathbf{k}$. The expected value and variance of the signal is

$$E\left[\tilde{\Phi}_{j,n}\right] = \Phi_{j,n}, \tag{A3}$$

$$\mathrm{Var}\left[\tilde{\Phi}_{j,n}\right] = \sigma^2. \tag{A4}$$

When stochastic variables are is uncorrelated, the expected value operator is linear and multiplicative, i.e. $E[XY] = E[X]E[Y]$, while the variance operator is linear and follows $\mathrm{Var}[XY] = |E[X]|^2\mathrm{Var}[Y] + |E[Y]|^2\mathrm{Var}[X] + \mathrm{Var}[X]\mathrm{Var}[Y]$. This applies also to complex random variables (O'Donoughue and Moura, 2012). As such, the moments of a spatial cross correlation of Eq. A2 integrated over time are

$$\begin{aligned} E\left[\sum_{n=1}^{N_t} \tilde{\Phi}_{j,n}\tilde{\Phi}^*_{l,n}\right] &= \sum_{n=1}^{N_t} E\left[\tilde{\Phi}_{j,n}\right] E\left[\tilde{\Phi}^*_{l,n}\right] = \\ &= N_t A^2 e^{-i(\langle \mathbf{k}, \mathbf{r}_j - \mathbf{r}_l \rangle_{\mathbb{R}^3}}, \end{aligned} \tag{A5}$$

$$\begin{aligned} &\mathrm{Var}\left[\sum_{n=1}^{N_t} \tilde{\Phi}_{j,n}\tilde{\Phi}^*_{l,n}\right] = \sum_{n=1}^{N_t} \mathrm{Var}\left[\tilde{\Phi}_{j,n}\tilde{\Phi}^*_{l,n}\right] = \\ &= \sum_{n=1}^{N_t} \left|E\left[\tilde{\Phi}_{j,n}\right]\right|^2 \mathrm{Var}\left[\tilde{\Phi}^*_{l,n}\right] + \left|E\left[\tilde{\Phi}^*_{l,n}\right]\right|^2 \mathrm{Var}\left[\tilde{\Phi}_{j,n}\right] \\ &+ \mathrm{Var}\left[\tilde{\Phi}_{j,n}\right] \mathrm{Var}\left[\tilde{\Phi}^*_{l,n}\right] = N_t(2A^2\sigma^2 + \sigma^4). \end{aligned} \tag{A6}$$

https://doi.org/10.5194/amt-2020-220
Preprint. Discussion started: 18 September 2020

Atmospheric Measurement Techniques Discussions

The expected noise power is given by the noisy signal variance when $A = 0$, i.e $P_{\text{Noise}} = N_t\sigma^4$. Therefore, the "SNR" for a cross correlated signal would be defined as

$$\frac{\left|E\left[\sum_{n=1}^{N_t}\tilde{\Phi}_{j,n}\tilde{\Phi}^*_{l,n}\right]\right|^2}{N_t\sigma^4} = \frac{N_t^2A^4}{N_t\sigma^4} = N_t\left(\frac{A}{\sigma}\right)^4. \tag{A7}$$

There is no standardized definition of coherent integration other then that such an integration should integrate the quadrature components of the signal envelope by taking phase into account (e.g Miller and Bernstein, 1957). As the phases of the cross correlation signal are preserved by the temporal integration of cross correlations, it is essentially the cross correlation envelope that is integrated. I.e., as the component $e^{-i(\langle\mathbf{k},\mathbf{r}_j-\mathbf{r}_l\rangle_{\mathbb{R}^3}}$ does not change, a simple summation can be referred to as coherent integration. However, a more efficient coherent integration would be to apply a matched filter integration prior to cross correlation.

Assuming a matched filter has perfectly modeled the temporal component of the signal ϕ_n, the statistical moments of the cross correlation of the matched filter integration would be

$$\begin{aligned}
&E\left[\left(\sum_{n=1}^{N_t}\tilde{\Phi}_{j,n}e^{-i\phi_n}\right)\left(\sum_{m=1}^{N_t}\tilde{\Phi}^*_{l,m}e^{i\phi_m}\right)\right] = \\
&= \sum_{n=1}^{N_t}\sum_{m=1}^{N_t} E\left[(Ae^{-i\langle\mathbf{k},\mathbf{r}_j\rangle_{\mathbb{R}^3}} + \xi_{j,n})(Ae^{i\langle\mathbf{k},\mathbf{r}_l\rangle_{\mathbb{R}^3}} + \xi_{l,m})\right] = \\
&= \sum_{n=1}^{N_t}\sum_{m=1}^{N_t} A^2e^{-i\langle\mathbf{k},\mathbf{r}_j-\mathbf{r}_l\rangle_{\mathbb{R}^3}} = \\
&= N_t^2A^2e^{-i\langle\mathbf{k},\mathbf{r}_j-\mathbf{r}_l\rangle_{\mathbb{R}^3}},
\end{aligned} \tag{A8}$$

$$\begin{aligned}
&\mathrm{Var}\left[\left(\sum_{n=1}^{N_t}\tilde{\Phi}_{j,n}e^{-i\phi_n}\right)\left(\sum_{m=1}^{N_t}\tilde{\Phi}^*_{l,m}e^{i\phi_m}\right)\right] = \\
&= \sum_{n=1}^{N_t}\sum_{m=1}^{N_t} \mathrm{Var}\left[(Ae^{-i\langle\mathbf{k},\mathbf{r}_j\rangle_{\mathbb{R}^3}} + \xi_{j,n})(Ae^{i\langle\mathbf{k},\mathbf{r}_l\rangle_{\mathbb{R}^3}} + \xi_{l,m})\right] = \\
&= \sum_{n=1}^{N_t}\sum_{m=1}^{N_t} 2A^2\sigma^2 + \sigma^4 \\
&= N_t^2(2A^2\sigma^2 + \sigma^4).
\end{aligned} \tag{A9}$$

Here we have used the fact that complex rotations of ξ does not affect the distribution as it is circularly symmetrical. This shows that a perfect matched filter integration prior to cross correlation would produce a more effective coherent integration. The "SNR" for the latter cross correlated signal is

$$\frac{N_t^4A^4}{N_t^2\sigma^4} = N_t^2\left(\frac{A}{\sigma}\right)^4. \tag{A10}$$

The SKiYMET system does not transmit coded pulses and the scope of this paper was not to develop a new analysis pipeline. Therefore, we have not implemented a matched filter integration routine.

Author contributions. Daniel Kastinen developed the analysis and model code and performed the simulations and data analysis. Alexander Kozlovsky provided the data set analysed. Daniel Kastinen prepared the manuscript with contributions from Johan Kero and Alexander Kozlovsky. All the authors contributed to proof reading the manuscript.

Competing interests. No competing interests are present.

https://doi.org/10.5194/amt-2020-220
Preprint. Discussion started: 18 September 2020

References

Bianchi, C. and Meloni, A.: Natural and man-made terrestrial electromagnetic noise: an outlook, Annals of geophysics, 50, 435–445, 2007.

Brown, P., Spalding, R. E., ReVelle, D. O., Tagliaferri, E., and Worden, S. P.: The flux of small near-Earth objects colliding with the Earth, Nature, 420, 294–296, https://doi.org/10.1038/nature01238, 2002.

Ceplecha, Z., Borovička, J., Elford, W. G., Revelle, D. O., Hawkes, R. L., Porubčan, V., and Šimek, M.: Meteor Phenomena and Bodies, Space Science Reviews, 84, 327–471, https://doi.org/10.1023/A:1005069928850, 1998.

Chau, J. L. and Clahsen, M.: Empirical Phase Calibration for Multistatic Specular Meteor Radars Using a Beamforming Approach, Radio Science, 54, 60–71, https://doi.org/10.1029/2018RS006741, 2019.

Gaensler, B. M.: Radio Emission from the Milky Way, in: Milky Way Surveys: The Structure and Evolution of our Galaxy, edited by Clemens, D., Shah, R., and Brainerd, T., vol. 317 of *Astronomical Society of the Pacific Conference Series*, p. 217, 2004.

Hanley, J. A. and Lippman-Hand, A.: If nothing goes wrong, is everything all right?: interpreting zero numerators, Jama, 249, 1743–1745, 1983.

Hocking, W. K.: A new approach to momentum flux determinations using SKiYMET meteor radars, Ann. Geophys., 23, 2433–2439, https://doi.org/10.5194/angeo-23-2433-2005, https://www.ann-geophys.net/23/2433/2005/, 2005.

Hocking, W. K., Fuller, B., and Vandepeer, B.: Real-time determination of meteor-related parameters utilizing modern digital technology, Journal of Atmospheric and Solar-Terrestrial Physics, 63, 155–169, https://doi.org/10.1016/S1364-6826(00)00138-3, 2001.

Holdsworth, D. A.: Angle of arrival estimation for all-sky interferometric meteor radar systems, Radio Sci., 40, RS6010, https://doi.org/10.1029/2005RS003245, 2005.

Holdsworth, D. A., Reid, I. M., and Cervera, M. A.: Buckland Park all-sky interferometric meteor radar, Radio Sci., 39, RS5009, https://doi.org/10.1029/2003RS003014, 2004.

Jones, J., Webster, A. R., and Hocking, W. K.: An improved interferometer design for use with meteor radars, Radio Science, 33, 55–65, https://doi.org/10.1029/97RS03050, 1998.

Kastinen, D. and Kero, J.: A Monte Carlo-type simulation toolbox for Solar System small body dynamics: Application to the October Draconids, Planetary and Space Science, 143, 53–66, https://doi.org/10.1016/j.pss.2017.03.007, 2017.

Kastinen, D. and Kero, J.: Probabilistic analysis of ambiguities in radar echo direction of arrival from meteors, Atmospheric Measurement Techniques Discussions, 2020, 1–48, https://doi.org/10.5194/amt-2020-157, https://www.atmos-meas-tech-discuss.net/amt-2020-157/, 2020.

Kero, J., Campbell-Brown, M. D., Stober, G., Chau, J. L., Mathews, J. D., and Pellinen-Wannberg, A.: Radar Observations of Meteors, p. 65, 2019.

Miller, K. and Bernstein, R.: An analysis of coherent integration and its application to signal detection, IRE Transactions on Information Theory, 3, 237–248, https://doi.org/10.1109/TIT.1957.1057425, 1957.

O'Donoughue, N. and Moura, J. M. F.: On the Product of Independent Complex Gaussians, IEEE Transactions on Signal Processing, 60, 1050–1063, 2012.

Papoulis, A. and Pillai, S. U.: Probability, random variables, and stochastic processes, Tata McGraw-Hill Education, 2002.

Plane, J. M.: Atmospheric chemistry of meteoric metals, Chemical reviews, 103, 4963–4984, 2003.

Plane, J. M.: Cosmic dust in the Earth's atmosphere, Chemical Society Reviews, 41, 6507–6518, 2012.

Polisensky, E.: LFmap: A low frequency sky map generating program, Long Wavelength Array Memo Series, 111, 2007.

https://doi.org/10.5194/amt-2020-220
Preprint. Discussion started: 18 September 2020

Atmospheric Measurement Techniques Discussions
Open Access

Schmidt, R. O.: Multiple emitter location and signal parameter estimation, IEEE Transactions on Antennas and Propagation, 34, 276–280, https://doi.org/10.1109/TAP.1986.1143830, 1986.

Vaubaillon, J., Colas, F., and Jorda, L.: A new method to predict meteor showers. I. Description of the model, Astronomy and Astrophysics, 439, 751–760, https://doi.org/10.1051/0004-6361:20041544, 2005a.

Vaubaillon, J., Colas, F., and Jorda, L.: A new method to predict meteor showers. II. Application to the Leonids, Astronomy and Astrophysics, 439, 761–770, https://doi.org/10.1051/0004-6361:20042626, 2005b.

Vierinen, J., Chau, J. L., Pfeffer, N., Clahsen, M., and Stober, G.: Coded continuous wave meteor radar, 2016.

Wiegert, P., Vaubaillon, J., and Campbell-Brown, M.: A dynamical model of the sporadic meteoroid complex, Icarus, 201, 295–310, https://doi.org/10.1016/j.icarus.2008.12.030, 2009.

Younger, J. P. and Reid, I. M.: Interferometer angle-of-arrival determination using precalculated phases, Radio Sci., 52, 1058–1066, https://doi.org/10.1002/2017RS006284, 2017.